

Article

Mechanical Strength and Energy Absorption Optimization of Biomimetic Honeycomb Anti-Collision Pier

Jianjun Wei ¹, Yufei Wang ², Jiaqing Wang ³ , Xupei Yao ⁴, Di Wang ^{5,*}  and Xiangyu Wang ²

¹ School of Construction Engineering, Changzhou Vocational Institute of Engineering, Changzhou 213164, China

² School of Design and Built Environment, Curtin University, Perth, WA 6102, Australia

³ College of Civil Engineering, Nanjing Forestry University, Nanjing 210037, China

⁴ Department of Civil Engineering, Monash University, Clayton, VIC 3800, Australia

⁵ Institute for Smart City of Chongqing University in Liyang, Chongqing University, Changzhou 213300, China

* Correspondence: 202116131002@cqu.edu.cn

Abstract: The anti-collision pier plays an irreplaceable role in road traffic protection due to its significance. In this research, the biomimetic honeycomb structure was applied to internal anti-collision pier interior structures. The enhancement of mechanical strength and energy absorption characteristics was explored and optimized by five anti-collision pier honeycomb structures. Finite elements of the piers are designated as 650 mm in diameter and 850 mm in height. Polypropylene Acetate (PLA) material is utilized in this research due to its environment-friendly characteristics. Displacement loading in finite element simulation is 50 mm to the middle region of the model at YOZ direction. The energy-absorbing properties of five optimized honeycomb anti-collision piers at the same force position will be carefully compared. Moreover, the influence of internal hexagon direction-quantity configuration upon loading resistance under displacement loading is outlined. The results determined the best biomimetic structure to be three honeycomb shapes with a central triangle area, with maximum stress of 503.8 MPa and fracture displacement of 58.02 mm. Furthermore, the numerical simulation shows that the number of nest increases has a negative relationship with the effect upon force and deformation of the model. Moreover, the triangular central area is superior to the Y-shape central area in both mechanical strength and energy absorption performance.

Keywords: bionic structure optimization; road pier; numerical calculation; cellular structure



Citation: Wei, J.; Wang, Y.; Wang, J.; Yao, X.; Wang, D.; Wang, X. Mechanical Strength and Energy Absorption Optimization of Biomimetic Honeycomb Anti-Collision Pier. *Buildings* **2022**, *12*, 1941. <https://doi.org/10.3390/buildings12111941>

Academic Editor: Giovanni Minafo

Received: 7 September 2022

Accepted: 7 November 2022

Published: 10 November 2022

Publisher's Note: MDPI stays neutral with regard to jurisdictional claims in published maps and institutional affiliations.



Copyright: © 2022 by the authors. Licensee MDPI, Basel, Switzerland. This article is an open access article distributed under the terms and conditions of the Creative Commons Attribution (CC BY) license (<https://creativecommons.org/licenses/by/4.0/>).

1. Introduction

The anti-collision pier plays an irreplaceable role in traffic protection infrastructures, benefiting the turnouts, entrances, toll gates, and various dangerous sections of highways or urban roads [1,2]. Anti-collision piers demonstrate outstanding isolation, warning, and collision prevention functions. Specifically, when collisions inevitably take place upon vehicle and bifurcation/roadside guardrails, an anti-collision pier can also play the role of buffering item and the maximum impact energy can be absorbed to attenuate the injury to people and vehicles. Moreover, the structures effectively prevent the vehicles from running away off the road, avoiding secondary injury to the occupants as well as vehicles [3]. In conclusion, anti-collision piers play a very important role in reducing the degree of injury in traffic accidents.

However, the current structure of the crash pier cannot fulfill industry demand for the main reason that simple structures are required, limiting the effect of absorbing impact energy and offering insufficient protection for vehicle occupants [4,5]. First, the internal structure of the anti-collision pier should obtain a certain degree of contractible elasticity, which ensures the maximum resistance of pier buffering displacement before fracture [6]. On this basis, the internal pier body is recommended to be formed as a grille element to ensure sufficient shape contraction with maximized impact energy absorption. Second, the

internal grille shape design is also critical when the pier is subjected to impact energy. For a typical triangular setting, the stable nature may lead to insufficient shrinking, eliminating impact energy absorption [7,8]. Meanwhile, the classical quadrilateral distribution yields a deformation tendency but results in pre-fracture deformation that cannot guarantee an effective buffering effect.

Bionic structures demonstrate outstanding energy-absorbing characteristics through their deformation when subjected to impact loads. Out of the varying range of bionic elements, the honeycomb structure can be a feasible solution due to its mechanical and energy absorption advantages. The honeycomb structure normally consists of single square hexagonal rooms arranged symmetrically back-to-back [9,10]. Such structures exhibit excellent geometrical and mechanical properties such as high strength and light weight [11]. Pan et al. [12] introduced a new energy absorption device into the design of anti-collision structures, which consisted of a 'U' shaped thin-walled steel plate with GFRP (Glass Fiber Reinforced Plastic) honeycomb filling. Moreover, the bionic honeycomb structures also demonstrated desirable sound insulation, thermal insulation, and energy absorption, and are therefore widely used in aerospace, construction, and material fields [13]. In this project, the biomimetic honeycomb anti-collision pier will be constructed using 3D printing technology.

There are numerous studies on the relationship between the honeycomb inertia configuration and energy absorption performance [14]. Hu et al. [15] divided the energy absorption for honeycomb structures into three parts, which were plastic energy dissipated by the plastic hinge, kinetic collision energy, and inertia energy between the cell walls. Niu et al. [16] compared numerical simulations and experimental analyses of traditional honeycomb structures (square triangle, rhombus, hexagon, etc.) and combined honeycomb (Kagome). The team found the honeycomb shape and configuration exert a great impact on the overall deformation pattern of the honeycomb structures. Meanwhile, Zhang et al. [17] determined that the relative density resulted in varying destabilization and damage characteristics of aluminum honeycomb through numerical simulations. Zhang et al. [18] explored a novel square honeycomb structure which revealed an enhancement in loading resistance (69.6 kN), and energy absorption (1986.1 J).

In conclusion, the combination of bionic honeycomb elements and an anti-collision pier yields high porosity, stiffness, impact, and vibration resistance [19]. The structure can effectively improve energy absorption and alleviate the damage delivered to passengers, which provides a novel idea for crash pier optimization research [20–22]. In this paper, the honeycomb structure is applied to the crash pier with five varying internal structures. The finite element simulation is carried out to analyze the energy absorption effect of different honeycomb structure arrangements and numbers. The relationships of honeycomb configurations between force-deformation models will be fully explored.

2. Establishment of Finite Element Model

The finite element of the cylindrical collision pier is designated as 650 mm in diameter and 850 mm in height, following road traffic collision pier design specifications [23–25]. The anti-collision pier is made of Polypropylene Acetate (PLA) material, which is a novel bio-based and renewable biodegradable material. It exhibits outstanding biodegradability and can be completely degraded by microorganisms in nature under specific conditions after use, eventually generating carbon dioxide and water, and is recognized as an environmentally friendly material, suitable for the production of anti-collision piers [26].

Bionic structures exhibit great potential in architecture design, medical science, and aerospace engineering. The honeycomb structure consisting of regular hexagonal rooms is employed in this research of the desired energy-absorbing property when subjected to impact loads. Further, the outstanding properties of honeycomb structures—like high strength and light weight—could be further enhanced to optimize the cost and safety of traffic protection. Deformation and stress corresponding to the quantity and direction of regular hexagonal rooms will be analyzed by establishing finite element models. Five

models, considering three quantities and two angles, are designed in arranging regular hexagonal rooms (Figure 1). The hollow space for the five structures is strictly designed as equal, ensuring the same force volume. Meanwhile, the force–deformation behavior of the triangular-shaped central area and Y-shaped central area will be further analyzed.

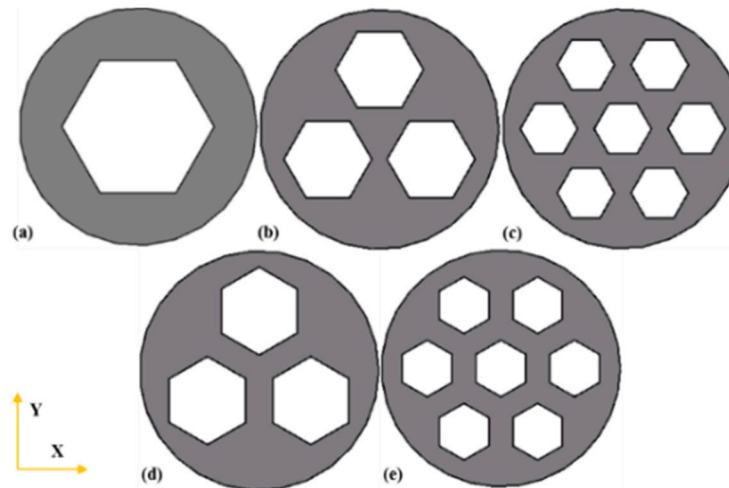


Figure 1. Internal structure configuration of honeycomb collision pier: (a) inscribing one concentric circle with a radius of 210 mm to propose one cut positive hexagon; (b) hollowing three circles out a radius of 121.24 mm (120° of distribution) to form internal square hexagons with a triangular-shaped central area; (c) inscribing seven circles at the radius of 79.38 mm at 60° distribution to produce the square hexagon along with a triangular-shaped central area; (d) rotate each square hexagon in (b) by 30° with center as the base point and terminally propose Y-shaped central area; (e) rotate each square hexagon in (c) by 30° to form Y-shaped central area.

Figure 2 demonstrates the model establishment at the XOY plane. The elements were stretched upward by 850 mm with a modulus of elasticity at 3500 MPa and Poisson's ratio at 0.35. The lower surface of the model is completely restrained to ensure no displacement rotation occurs in all directions. Enough displacement is necessary for clear deformation reflection of each area of the anti-collision piers. Displacement of 50 mm is the limit case considering the character of PLA material. Thus, 50 mm has been determined as the displacement loading in the finite element simulation. The impact position of the vehicle is roughly located at the middle height of the anti-collision pier. The specific loading position focused on the intersection range of the left-right offset of 100 mm in the YOZ plane and the upward offset of 325–525 mm in the XOY plane. Grids in the numerical modeling process in Abaqus are divided as 46 mm. The element type is determined as C3D8R, the eight-node linear hexahedral element. We use a static solver, ABAQUS/STANDARD, for the calculation of deformation and strain under impact loads. The elastic deformation of the impact load contact is first considered in the impact analysis in Abaqus. Then, Abaqus can calculate the plasticity and elastoplastic deformation, since calculations on plastic and plastic elastic step size in the simulation stage have been conducted. Finally, the deformation and strain will be output as the result. After displacement load simulations for the five models (a), (b), (c), (d) and (e), comparative analyses of different internal structures and different arrangements were carried out to explore the structural forms more applicable to the forces on the crash pier.

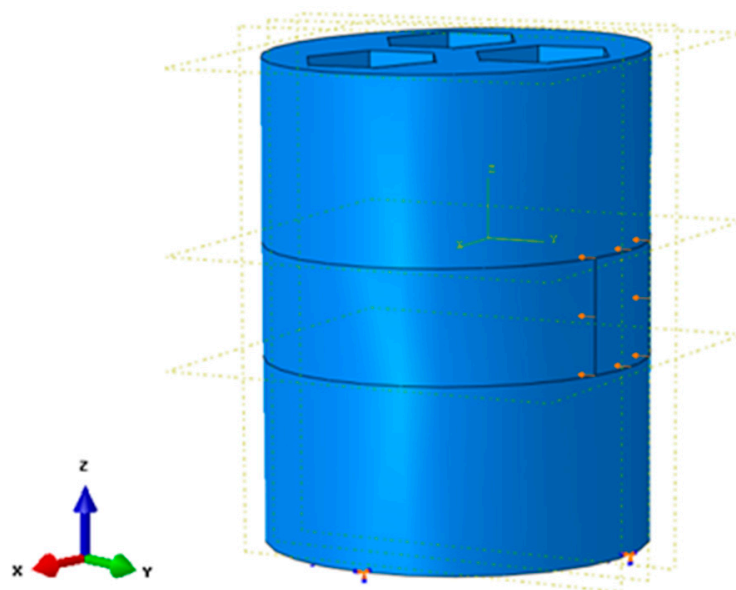


Figure 2. Schematic diagram of model loading.

3. Simulation Results and Discussion

3.1. Hexagon Quantity Comparison

Figure 3 describes the Mises stress cloud belonging to models (a), (b) and (c), with varying internal configurations subjected to the same displacement loads. The Mises stresses for models (a), (b) and (c) are 268.6 MPa, 503.8 MPa, and 348.0 MPa for the same displacement load of 50 mm, respectively. Model (b) demonstrates 87.6% and 44.8% higher maximum stress compared to models (a) and (c), which is the best crash pier element for force and structural optimization. Model (c) demonstrates 29.5% higher peak stress compared to model (a), ranking as the second optimized element. Furthermore, from the displacement cloud, the maximum displacements of models (a), (b) and (c) are 55.81 mm, 58.02 mm, and 55.45 mm, respectively, when subjected to a displacement load of 50 mm. Model (c) yields the smallest peak deformation compared to model (a) at 1.7% and model (b) at 4.7%. As a result, model (c) is more stable than its two counterparts for internal structural optimization. Moreover, the influence of hexagon quantity configuration upon fracture resistance is concluded. When the number of honeycombs inside the crash pier increases from three to seven, the effect of its internal arrangement on the structure will be eliminated, with a decreased Mises stress difference, from 9% to 3.2%.

The phenomenon is attributed to the number of internal honeycombs, that enhances the interaction between the honeycombs and the energy absorbing and deformation buffering effects [27]. However, after exceeding the threshold, the structure would turn into an over-dispersed phase, weakening its force performance. In conclusion, as the difference in deformation between model (c) and the other two models does not exceed 5%, model (b) is more suitable for the construction of crash piers, considering its 87.6% maximum stress advantages.

3.2. Hexagon Direction Comparison

The influence of internal hexagon direction upon loading resistance under displacement loading is outlined by comparing model (b)–(d) in Figure 4, and model (c)–(e) in Figure 5. For the three hexagons group, models (b) and (d) exhibit maximum stress at 503.8 MPa and 461.9 MPa, respectively. Model (b) is thus regarded as more reasonable for structural optimization compared with model (d). However, from the displacement cloud, the maximum displacement of model (d) stands at 57.67 mm, which is 1.4% smaller than model (b) when subjected to a displacement load of 50 mm; it can be seen that model (d) has a smaller peak value of deformation variables and is more stable compared to model (b)

for internal structural optimization. The load-displacement relationship curves of the five internal structures, along with the displacement up to 50 mm from 0 are shown in Figure 4. The inner boundary of the hexagons of models (b) and (c) is a triangular shape, while for models (d) and (e) it is a Y shape. The load of (b) and (c) is 98.437 kN and 105.914 kN when the displacement reaches 50 mm. However, the load of models (d) and (e) is 89.142 kN and 96.416 kN, respectively, significantly lower than models (b) and (c). It is concluded that when the inner boundary of the hexagons forms a triangular shape instead of a Y shape, the combined effect of force and deformation can be enhanced [28–30].

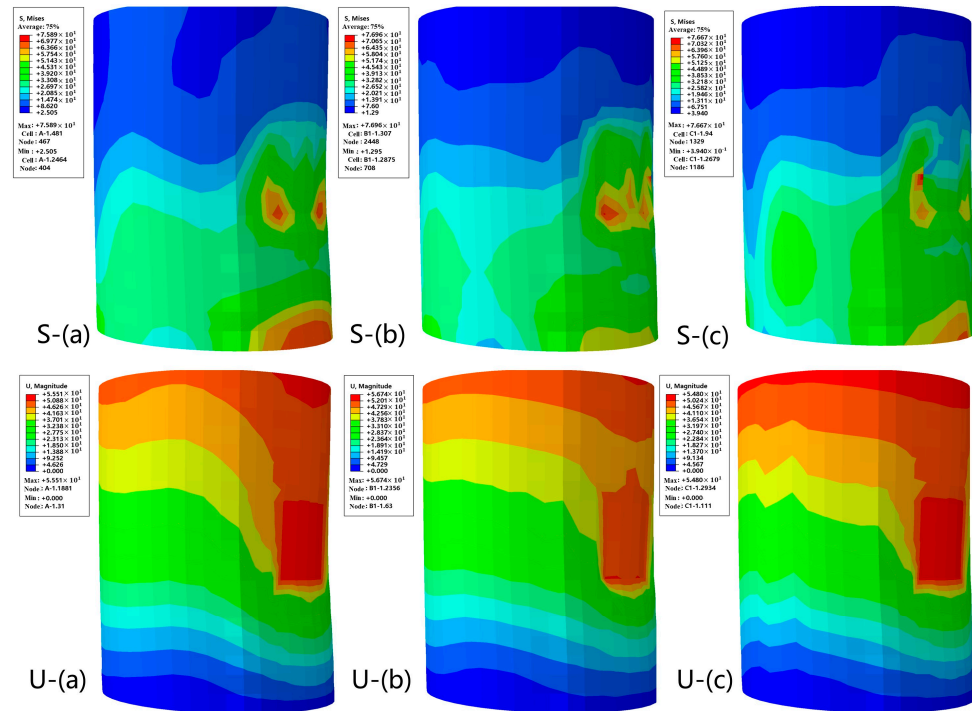


Figure 3. Displacement load clouds for models (a), (b) and (c).

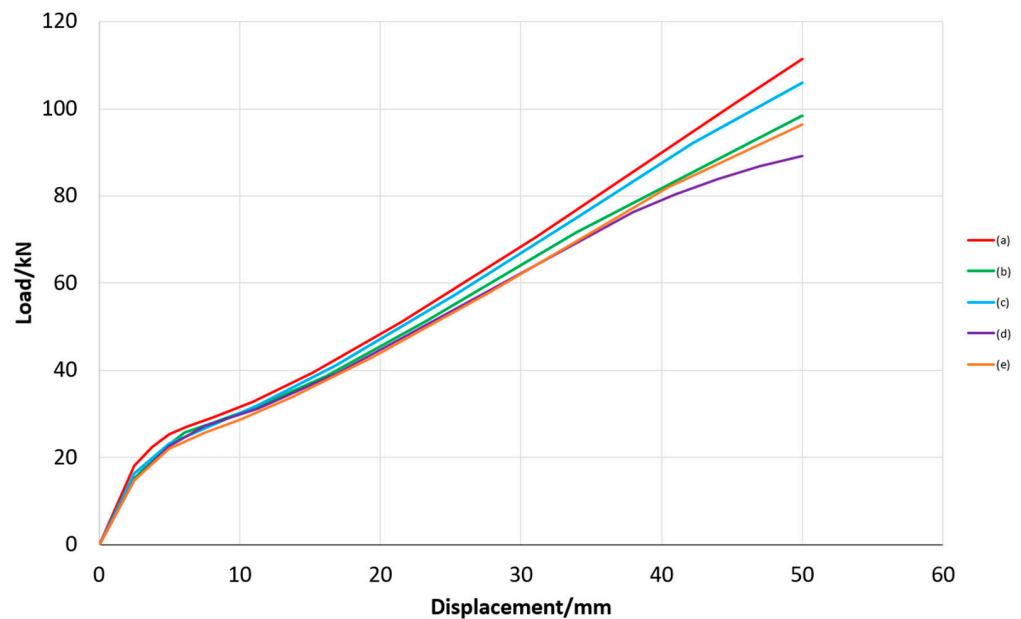


Figure 4. Load-displacement curves for models (a), (b), (c), (d) and (e).

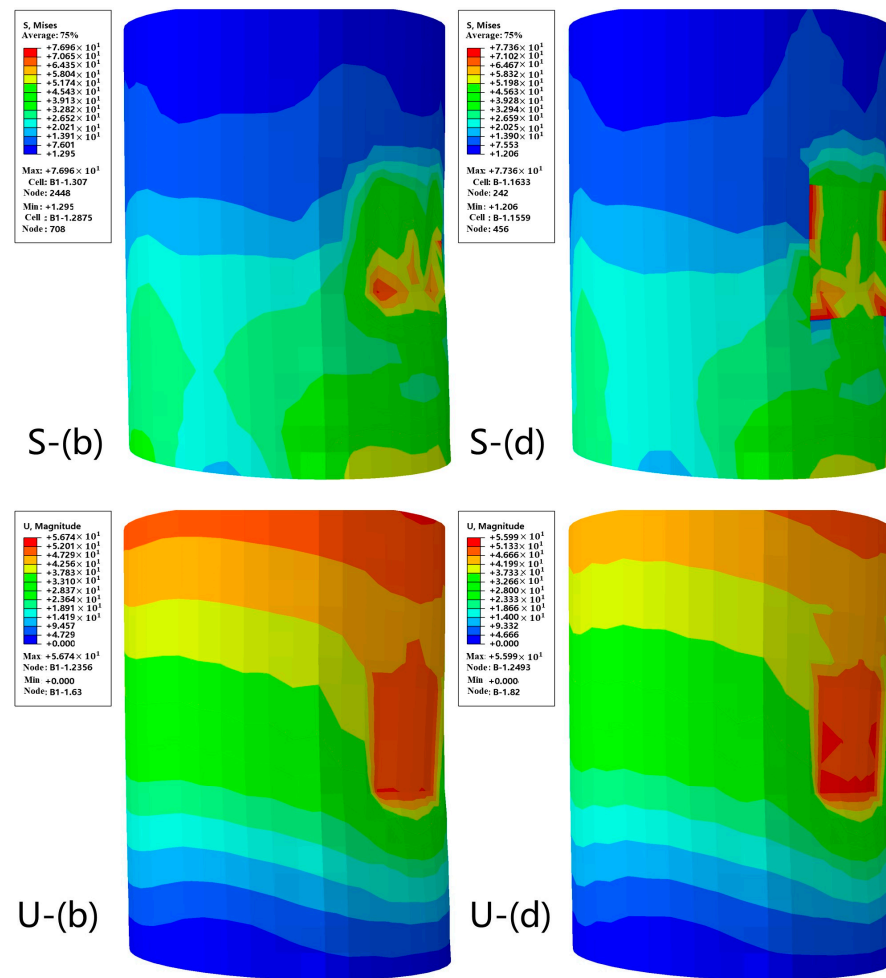


Figure 5. Displacement load clouds for models (b) and (d).

As shown in Figure 6, model (c) yields a maximum stress of 348.0 MPa, 11 MPa higher than model (e). However, model (e) obtains a 55.05 mm maximum displacement, which is 0.4 mm more than model (c) at 55.45 mm when subjected to a displacement load of 50 mm. In summary, model (e) has higher stress resistance and worse deformation performance and is more stable for internal structural optimization. The result verified the finding that when the solid central area is arranged in a triangular shape, the combined effect of force and deformation can be modified compared to a Y-shaped counterpart. This is because the solid triangular structure obtains outstanding stiffness toward fracture loading and deformation [31].

From these two sets of models, models (b) and (c) have higher stresses than those in models (d) and (e), respectively. However, they demonstrate higher peak deformation than their counterparts, which means the energy absorption potential is eliminated. This is because when the honeycombs of models (b) and (c) are arranged, a square triangle is formed at the boundary of each honeycomb, which enhances the overall stiffness, enhancing force resistance [31]. However, when the formation of such triangular cells is subjected to external loads, the deformation buffer effect between honeycombs is weakened and the overall deformation increases [32,33]. In addition, the three-hollowed-square-hexagons configuration with the triangular central area (model (b)) is regarded as the optimized honeycomb structure compared with all other models as it demonstrated the highest maximum stress at 503.8 MPa and moderate fracture displacement at 58.02 mm. In the future, artificial intelligence technology would be a promising tool in structural design and optimization [34,35].

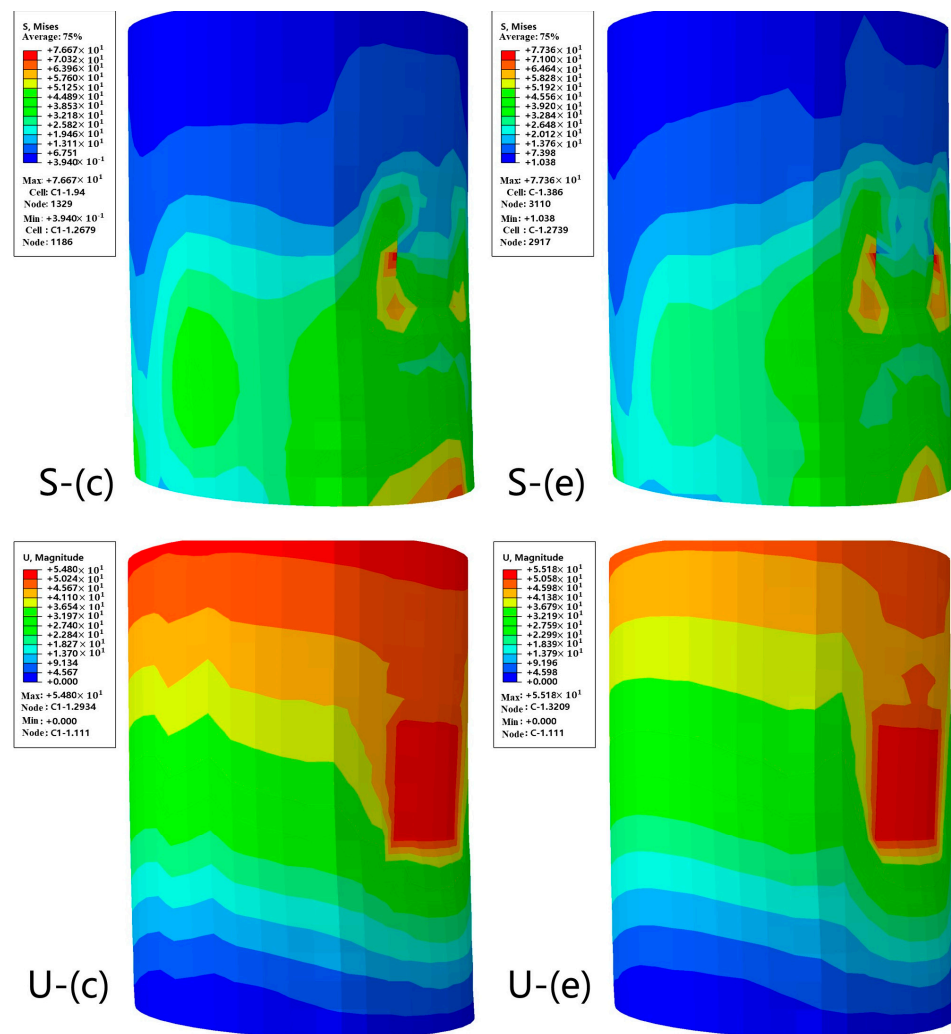


Figure 6. Displacement load clouds for models (c) and (e).

4. Conclusions

1. The honeycomb structure demonstrated outstanding energy-absorbing properties for the internal structure design of anti-collision piers, and can improve the cushioning effect of road impact prevention piers that are subjected to external forces, and reduce the hidden danger of road traffic.
2. Through the numerical calculation of all five models, model (b), with a three honeycomb shape with a central triangle area, obtained the best force-deformation behavior with maximum stress at 503.8 MPa and terminal displacement at 58.02 mm.
3. When the number of honeycombs inside the crash pier increases from three to seven, the effect of its internal arrangement on the structure will be eliminated, with a decreased Mises stress difference of 9% from 3.2%. As a result, the number of nest increases is in a negative relationship with the effect upon force and deformation of the model.
4. The numerical calculation of (b), (d) and (c), and (e) models with varying nest direction configurations show that the model is more stable in both mechanical strength and energy absorption performance when the central area is arranged in a triangle shape compared to a Y shape.

Author Contributions: Conceptualization, J.W. (Jianjun Wei) and X.W.; methodology, Y.W.; validation, J.W. (Jiaqing Wang) and X.Y.; writing—original draft preparation, D.W.; writing—review and editing, Y.W. and D.W. All authors have read and agreed to the published version of the manuscript.

Funding: This research received no external funding.

Conflicts of Interest: The authors declare no conflict of interest.

References

- Zhang, C.; Ali, A.; Sun, L. Investigation on low-cost friction-based isolation systems for masonry building structures: Experimental and numerical studies. *Eng. Struct.* **2021**, *243*, 112645. [[CrossRef](#)]
- Liu, B.; Yang, S.; Li, W.; Zhang, M. Damping dissipation properties of rubberized concrete and its application in anti-collision of bridge piers. *Constr. Build. Mater.* **2020**, *236*, 117286. [[CrossRef](#)]
- Huang, H.; Huang, M.; Zhang, W.; Pospisil, S.; Wu, T. Experimental investigation on rehabilitation of corroded RC columns with BSP and HPFL under combined loadings. *J. Struct. Eng.* **2020**, *146*, 04020157. [[CrossRef](#)]
- Thomas, T.; Tiwari, G. Crushing behavior of honeycomb structure: A review. *Int. J. Crashworthiness* **2019**, *24*, 1–25. [[CrossRef](#)]
- Wang, Z.; Li, Z.; Zhou, W.; Hui, D. On the influence of structural defects for honeycomb structure. *Compos. Part B Eng.* **2018**, *142*, 183–192. [[CrossRef](#)]
- Zhang, W.; Zhang, R.; Han, L.; Goh, A. Engineering properties of Bukit Timah Granitic residual soils in Singapore DTL2 braced excavations. *Undergr. Space* **2019**, *4*, 98–108. [[CrossRef](#)]
- Zhou, C.; Wang, J.; Jia, W.; Fang, Z. Torsional behavior of ultra-high performance concrete (UHPC) rectangular beams without steel reinforcement: Experimental investigation and theoretical analysis. *Compos. Struct.* **2022**, *299*, 116022. [[CrossRef](#)]
- Wu, C.; Hong, L.; Wang, L.; Zhang, R.; Pijush, S.; Zhang, W. Prediction of wall deflection induced by braced excavation in spatially variable soils via convolutional neural network. *Gondwana Res.* **2022**, *In Press*.
- Lubis, S.; Siregar, A.M.; Siregar, I. Study of Statically Tested Honeycomb Structure. *Int. J. Econ. Technol. Soc. Sci.* **2021**, *2*, 1–12.
- Zhang, Q.; Yang, X.; Li, P.; Huang, G.; Feng, S.; Shen, C.; Han, B.; Zhang, X.; Jin, F.; Xu, F. Bioinspired engineering of honeycomb structure—Using nature to inspire human innovation. *Prog. Mater. Sci.* **2015**, *74*, 332–400. [[CrossRef](#)]
- Sun, J.; Lin, S.; Zhang, G.; Sun, Y.; Zhang, J.; Chen, C.; Morsy, A.M.; Wang, X. The effect of graphite and slag on electrical and mechanical properties of electrically conductive cementitious composites. *Constr. Build. Mater.* **2021**, *281*, 122606. [[CrossRef](#)]
- Pan, J.; Fang, H.; Xu, M.C.; Wu, Y.F. Study on the performance of energy absorption structure of bridge piers against vehicle collision. *Thin-Walled Struct.* **2018**, *130*, 85–100. [[CrossRef](#)]
- Zhang, W.; Gu, X.; Han, L.; Wu, J.; Xiao, Z.; Liu, M.; Wang, L. A short review of probabilistic slope stability analysis considering spatial variability of geomaterial parameters. *Innov. Infrastruct. Solut.* **2022**, *7*, 1–21. [[CrossRef](#)]
- Sun, J.; Wang, Y.; Li, K.; Yao, X.; Zhu, B.; Wang, J.; Dong, Q.; Wang, X. Molecular interfacial properties and engineering performance of conductive fillers in cementitious composites. *J. Mater. Res. Technol.* **2022**, *19*, 591–604. [[CrossRef](#)]
- Hu, L.; Yu, T. Influence of inertia effect on the energy absorption of hexagonal honeycombs. *Binggong Xuebao/Acta Armamentarii* **2009**, *30*, 24.
- Niu, B.; Wang, B. Directional mechanical properties and wave propagation directionality of Kagome honeycomb structures. *Eur. J. Mech. A/Solids* **2016**, *57*, 45–58. [[CrossRef](#)]
- Zhang, S.; Chen, W.; Gao, D.; Xiao, L.; Han, L. Experimental study on dynamic compression mechanical properties of aluminum honeycomb structures. *Appl. Sci.* **2020**, *10*, 1188. [[CrossRef](#)]
- Zhang, L.; Xie, Z.; Li, J.; Zhang, J.; Yu, Q.; Zhang, C. A new polyurethane-steel honeycomb composite pier anti-collision device: Concept and compressive behavior. *Adv. Struct. Eng.* **2022**, *25*, 820–836. [[CrossRef](#)]
- Zhang, G.; Wang, J.; Jiang, Z.; Peng, C.; Sun, J.; Wang, Y.; Chen, C.; Morsy, A.M.; Wang, X. Properties of Sustainable Self-Compacting Concrete containing Activated Jute Fiber and Waste Mineral Powders. *J. Mater. Res. Technol.* **2022**, *19*, 1740–1758. [[CrossRef](#)]
- Zhang, G.; Chen, C.; Sun, J.; Li, K.; Xiao, F.; Wang, Y.; Chen, M.; Huang, J.; Wang, X. Mixture optimisation for cement-soil mixtures with embedded GFRP tendons. *J. Mater. Res. Technol.* **2022**, *18*, 611–628. [[CrossRef](#)]
- Sun, J.; Wang, J.; Zhu, Z.; He, R.; Peng, C.; Zhang, C.; Huang, J.; Wang, Y.; Wang, X. Mechanical Performance Prediction for Sustainable High-Strength Concrete Using Bio-Inspired Neural Network. *Buildings* **2022**, *12*, 65. [[CrossRef](#)]
- Huang, H.; Guo, M.; Zhang, W.; Huang, M. Seismic Behavior of Strengthened RC Columns under Combined Loadings. *J. Bridge Eng.* **2022**, *27*, 05022005. [[CrossRef](#)]
- Uğur, L.; Duzcukoglu, H.; Sahin, O.S.; Akkuş, H. Investigation of impact force on aluminium honeycomb structures by finite element analysis. *J. Sandw. Struct. Mater.* **2020**, *22*, 87–103. [[CrossRef](#)]
- Ahmed, N.; Xue, P. Governing the in-plane axial crushing of honeycomb with regular hexagonal symmetric division cells using cross-hinge inserts. *Int. J. Mech. Sci.* **2019**, *161*, 105062. [[CrossRef](#)]
- Sethi, N.; Ahlawat, S. Low-fidelity Design Optimization and Development of a VTOL Swarm UAV using an Open-source Framework. *Array* **2022**, *14*, 100183. [[CrossRef](#)]
- Bai, Y.; Yu, K.; Zhao, J.; Zhao, R. Experimental and simulation investigation of temperature effects on modal characteristics of composite honeycomb structure. *Compos. Struct.* **2018**, *201*, 816–827. [[CrossRef](#)]

27. Wang, J.J.; Song, Y.C.; Wang, W.; Chen, C.J. Evaluation of flexible floating anti-collision device subjected to ship impact using finite-element method. *Ocean Eng.* **2019**, *178*, 321–330. [[CrossRef](#)]
28. Foo, C.C.; Chai, G.B.; Seah, L.K. Mechanical properties of Nomex material and Nomex honeycomb structure. *Compos. Struct.* **2007**, *80*, 588–594. [[CrossRef](#)]
29. Miura, Y.; Hirai, R.; Kobayashi, Y.; Sato, M. Spin-gap behavior of Na₃Cu₂SbO₆ with distorted honeycomb structure. *J. Phys. Soc. Jpn.* **2006**, *75*, 084707. [[CrossRef](#)]
30. Choi, W.-H.; Kim, C.-G. Broadband microwave-absorbing honeycomb structure with novel design concept. *Compos. Part B Eng.* **2015**, *83*, 14–20. [[CrossRef](#)]
31. Pan, J.; Fang, H.; Xu, M.C.; Xue, X.Z. Dynamic performance of a sandwich structure with honeycomb composite core for bridge pier protection from vehicle impact. *Thin-Walled Struct.* **2020**, *157*, 107010. [[CrossRef](#)]
32. Cheng, H.; Sun, L.; Wang, Y.; Chen, X. Effects of actual loading waveforms on the fatigue behaviours of asphalt mixtures. *Int. J. Fatigue* **2021**, *151*, 106386. [[CrossRef](#)]
33. Cheng, H.; Liu, L.; Sun, L. Bridging the gap between laboratory and field moduli of asphalt layer for pavement design and assessment: A comprehensive loading frequency-based approach. *Front. Struct. Civ. Eng.* **2022**, *16*, 267–280. [[CrossRef](#)]
34. Sun, J.; Ma, Y.; Li, J.; Zhang, J.; Ren, Z.; Wang, X. Machine learning-aided design and prediction of cementitious composites containing graphite and slag powder. *J. Build. Eng.* **2021**, *43*, 102544. [[CrossRef](#)]
35. Feng, W.; Wang, Y.; Sun, J.; Tang, Y.; Wu, D.; Jiang, Z.; Wang, J.; Wang, X. Prediction of thermo-mechanical properties of rubber-modified recycled aggregate concrete. *Constr. Build. Mater.* **2022**, *318*, 125970. [[CrossRef](#)]